THROMBOSIS AND HEMOSTASIS

Expression of a structurally constrained von Willebrand factor variant triggers acute thrombotic thrombocytopenic *purpura* in mice

Yoko Morioka,[1] Caterina Casari,[2] Nikolett Wohner,[2] Sungyun Cho,[3] Sachiko Kurata,[1] Ayumi Kitano,[1] Olivier D. Christophe,[2] Peter J. Lenting,[2] Renhao Li,[3] Cécile V. Denis,[2] and Nicolas Prévost[1]

[1]Kyoto University, Career-Path Unit for Young Life Scientists, Kyoto, Japan; [2]Inserm Unité 770, Université Paris-Sud, Unité Mixte de Recherche-S 770, Le Kremlin-Bicêtre, France; and [3]Aflac Cancer and Blood Disorders Center, Department of Pediatrics, Emory University School of Medicine, Atlanta, GA

Key Points

- Introduction of a disulfide bond within the A2 domain renders VWF highly thrombogenic and resistant to proteolysis.
- Expression of mVWF/p.S1494C-p.A1534C in mice triggers an acute onset of thrombotic thrombocytopenic *purpura*.

Thrombotic thrombocytopenic *purpura* (TTP) is a life-threatening disease that presents with thrombocytopenia, disseminated thrombosis, hemolytic anemia, and organ dysfunction. The etiology of TTP has revealed that patients share a deficiency in plasma protease a disintegrin and metalloproteinase with a thrombospondin type 1 motif, member 13 (ADAMTS13), the enzyme responsible for cleaving ultra-large von Willebrand factor (VWF) multimers into nonthrombogenic fragments. Therefore, existing TTP mouse models were developed by targeted disruption of the *ADAMTS13* gene. ADAMTS13$^{-/-}$ mice are mostly asymptomatic in the absence of a trigger, as redundant proteases appear to take on VWF processing. As an alternative approach to creating one such model, we devised a strategy based on the expression of a cleavage-resistant VWF mutant in mice. The creation of a disulfide bond within the A2 domain of VWF was found to render VWF multimers resistant to proteolysis by plasma proteases under flow. Furthermore, mice expressing the murine VWF/p.S1494C-p.A1534C mutant present with symptoms characteristics of acute TTP such as thrombocytopenia, red cell shredding, accumulation of VWF-rich thrombi in the microvasculature, and advanced TTP symptoms such as renal dysfunction and splenomegaly. Because this model appears to faithfully emulate the pathophysiology of TTP, it should prove most useful in the study of microangiopathic diseases and their treatment. (*Blood*. 2014;123(21):3344-3353)

Introduction

Thrombotic thrombocytopenic *purpura* (TTP) is a rarely occurring human disease with a high mortality rate when left untreated (90%). TTP is due to a deficiency in plasma protease a disintegrin and metalloproteinase with a thrombospondin type 1 motif, member 13 (ADAMTS13) whose sole known substrate is von Willebrand factor (VWF).[1,2] VWF is a large multidomain plasma protein produced by endothelial cells and megakaryocytes in the form of ultra-large (UL) prothrombotic multimers (UL-VWF). In the absence of ADAMTS13, UL-VWF multimers remain uncleaved and form long endothelium-tethered strings that capture and cause platelets to form large aggregates in conditions of high shear rate.[3] These disseminated thrombi can accumulate in the microvasculature and cause organs to fail.[4] TTP is clinically defined as a combination of thrombocytopenia, hemolytic anemia, and organ dysfunction (kidneys and brain in particular) due to the presence of VWF-rich thrombi in their venulae and arterioles.[5] One of the reasons why our understanding of TTP remains fragmentary is the absence of an animal model of early- and late-stage TTP. A number of research teams have produced murine and primate models of TTP, with various degrees of success.[6] Of note, ADAMTS13-deficient mice do not spontaneously develop TTP,[7] or only sporadically,[8] suggesting that the cleavage of UL-VWF multimers may involve >1 enzyme in mice. To circumvent the challenges of a multiprotease-targeted approach to creating a mouse model of TTP, we opted for a simpler strategy and developed a cleavage-resistant VWF variant. Because VWF cleavage by ADAMTS13 requires the unfolding of its A2 domain by blood flow forces,[9,10] we hypothesized that a strategically placed disulfide bridge within A2 may render VWF resistant to elongational forces and proteolysis. The studies presented hereafter show that the expression of 1 such structurally constrained VWF mutant can elicit a rapid onset of acute TTP in mice.

Methods

A comprehensive account of all cloning, staining, and biochemical procedures has been included in the supplemental Data available on the *Blood* Web site. All experiments were performed in strict compliance with Kyoto University guidelines on recombinant DNA experiments and animal experiments, as well as the regulations of the Ministry of Environment, the Ministry of Education, Culture, Sports, Science and Technology, the Ministry of Finance, Ministry of Health, Labor and Welfare, Ministry of Agriculture,

Submitted October 26, 2013; accepted April 2, 2014. Prepublished online as *Blood* First Edition paper, April 8, 2014; DOI 10.1182/blood-2013-10-531392.

Y.M. and C.C. contributed equally to this work.

The online version of this article contains a data supplement.

The publication costs of this article were defrayed in part by page charge payment. Therefore, and solely to indicate this fact, this article is hereby marked "advertisement" in accordance with 18 USC section 1734.

Forestry and Fisheries of Japan, Ministry of Economy, Trade and Industry, and the Ministry of the Environment. This study was conducted in accordance with the Declaration of Helsinki.

Reagents

Unless stated otherwise, all reagents and chemicals were manufactured by Nacalai Tesque (Kyoto, Japan). All secondary antibodies were purchased from Jackson Immunoresearch (West Grove, PA).

Determination of murine VWF (mVWF) levels by ELISA

Plasma VWF concentrations are measured as described previously.[11] Plasma VWF levels from normal C57Bl/6 mice was used as reference, and values are expressed as a percentage of (measured VWF)/(reference VWF). Concentrated supernatant containing VWF/WT or VWF/p.S1494C-p.S1534C were used in the nanobody AU/VWFa-11-based assay to test their GpIb-binding conformation.[12]

Flow assay

On day 1, HA-HRH1 HEK293T were plated on poly-L-lysine-coated $I^{0.4}$ Luer μ-slides (Ibidi, Martinsried, Germany) at a density of 10^5 cells/mL in complete Dulbecco's modified Eagle medium (DMEM). On day 2, cells were transfected with pCMV6-XL5-VWF constructs (Table 1). On day 3, complete DMEM was added to the cells. On the day of the experiment, cells were histamine treated and washed 1 time with complete DMEM. Two blood samples were collected from a healthy volunteer donor. One sample was anticoagulated with 6× ACD (65 mM trisodium citrate, 70 mM citric acid, and 100 mM dextrose, pH = 4.4) and the second sample with 150 U/mL heparin (heparin does not interfere with VWF cleavage by ADAMTS13 and may even increase it[13]). Plasma-free blood was prepared from the ACD-anticoagulated sample and resuspended in 50 g/L bovine serum albumin *N*-2-hydroxyethylpiperazine-*N*′-2-ethanesulfonic acid-Tyrode's buffer as described in Savage et al.[14] Both plasma-free and heparinized blood samples were then labeled with 10 μM mepacrine for 30 minutes at 37°C. $I^{0.4}$ Luer μ-slide chambers were connected to a PHD4400 syringe pump (Harvard Apparatus, Holliston, MA) equipped with a 100-mL syringe. For each chamber, 50 mL plasma-free blood was first flown in to locate platelet-decorated VWF strings. VWF string resistance to flow-induced cleavage was then assessed in 50 mL heparinized whole blood at shear rates of 1500 and 2500 seconds^{-1}. For each slide, 20 VWF string-containing fields were selected and monitored (through the use of a programmable stage).

Hydrodynamic injection

Tail vein injections were performed as described previously.[15] Briefly, VWF-null mice[16] were injected with 20 to 100 μg plasmid DNA in 154 mM NaCl (10% volume/weight ratio). Syringes (2.5- to 3-mL) fitted with a 261/2-gauge needle were used. Injections were performed in 5 seconds or less. Mice were included in the study that expressed VWF:Ag levels between 300% and 1000% compared with normal pooled mouse plasma, obtained from C57Bl/6 mice.

Results

VWF mutants (Table 1)

To create a proteolysis-resistant VWF variant, a number of cysteine codons were inserted in the A2 region of the VWF cDNA. Various positions were assessed using the Swiss-Pdb viewer software, and residues predicted to be stereochemically optimal for the formation of internal cross-links were systematically mutated. Serine 1494 and serine 1534 were among the residues selected for cysteine substitution, with the intent of forming a disulfide bond between the N-terminal ends of the β1 and β2 strands of the A2 domain of VWF (mutant VWF/p.S1494C-p.S1534C) (Figure 3A). Two control mutants bearing a single mutation were also engineered (mutants VWF/p.S1494C and VWF/p.S1534C).

Table 1. List of VWF constructs used in this study

Constructs		Purpose
pCMV6-XL5	h VWF/WT	Immunofluorescence/flow assay
	h VWF/p.S1494C	
	h VWF/p.S1534C	
	h VWF/p.S1494C-p.S1534C	
	Vn_{SP}-A2-His_6	Purification/proteolysis assays
	Vn_{SP}-A2/p.S1494C-p.S1534C-His_6	
pLIVE	mVWF/WT	Hydrodynamic injection in mice
	mVWF/p.S1494C-p.A1534C	

cDNA encoding either full-length human VWF or its A2 domain was subcloned into pCMV6-XL5, a plasmid that allowed better VWF expression in HEK293T cells than any other vector tested (data not shown). pLIVE constructs were done using the cDNA for mVWF. Of note, mVWF constructs bear a T103M mutation.

HA-HRH1 HEK293T cells as a model for VWF synthesis and secretion

A HEK293T cell line that stably expresses the human histamine receptor 1 was established (HA-HRH1 HEK293T). Transient transfection of VWF constructs in these cells leads to the formation of many Weibel-Palade body-like secretion granules (Figure 1A). On histamine treatment, HA-HRH1 HEK293T cells secrete these granules, and VWF multimers accumulate in dot-like surface microdomains similar to the ones observed in human umbilical vein endothelial cells[17] (Figure 1A). Sodium dodecyl sulfate (SDS)-agarose gel electrophoresis analysis of the supernatant of these cells confirmed the presence of various VWF protein multimers (Figure 1B). No difference in packaging and secretion was observed between native (wild-type [WT]) and mutant VWF. Moreover, VWF/WT and mutants were all produced as multimerized proteins (Figure 1).

Human VWF/p.S1494C-p.S1534C is resilient to cleavage by plasma proteases under flow and are highly prothrombotic

A flow-based experimental model was used to assess whether serine-to-cysteine VWF mutants are indeed impervious to the catalytic activity of blood proteases. HA-HRH1 HEK293T cells were grown and transfected inside poly-L-lysine-coated $I^{0.4}$ Luer μ-slides and subjected to histamine treatment. Cells were then exposed to a plasma-free blood cell suspension (no plasma protein) at a shear rate of 1500 seconds^{-1} to trigger the unfurling of ultra-large VWF multimers from the cell surface, without cleavage. Once platelet-decorated UL-VWF multimers were located in the chamber, video recording started, and whole blood (plasma proteases included) was then flown into the chamber at shear rates of 1500 and 2500 seconds^{-1}. As expected, UL-VWF strings from control cells were systematically severed within seconds (VWF/WT: 106 strings analyzed, VWF/p.S1494C: 68 strings analyzed, and VWF/p.S1534C: 61 strings analyzed) (Figure 2A-B; supplemental Videos). UL-VWF multimers bearing the p.S1494C-p.S1534C mutations (93 and 41 strings analyzed at 1500 and 2500 seconds^{-1}, respectively), on the contrary, did not undergo cleavage (observation period: 5 minutes at 1500 seconds^{-1} and 2.5 minutes at 2500 seconds^{-1} (Figure 2A-B; supplemental Videos). The double mutant was found to support the formation of unexpectedly large platelet aggregates. These platelet aggregates appear to initially distribute at somewhat regular intervals along the string axis instead of forming a continuous thrombus. We considered the possibility that the S1494C-S1534C double mutation induced an active Willebrand disease type 2B (VWD-type 2B)–like conformation

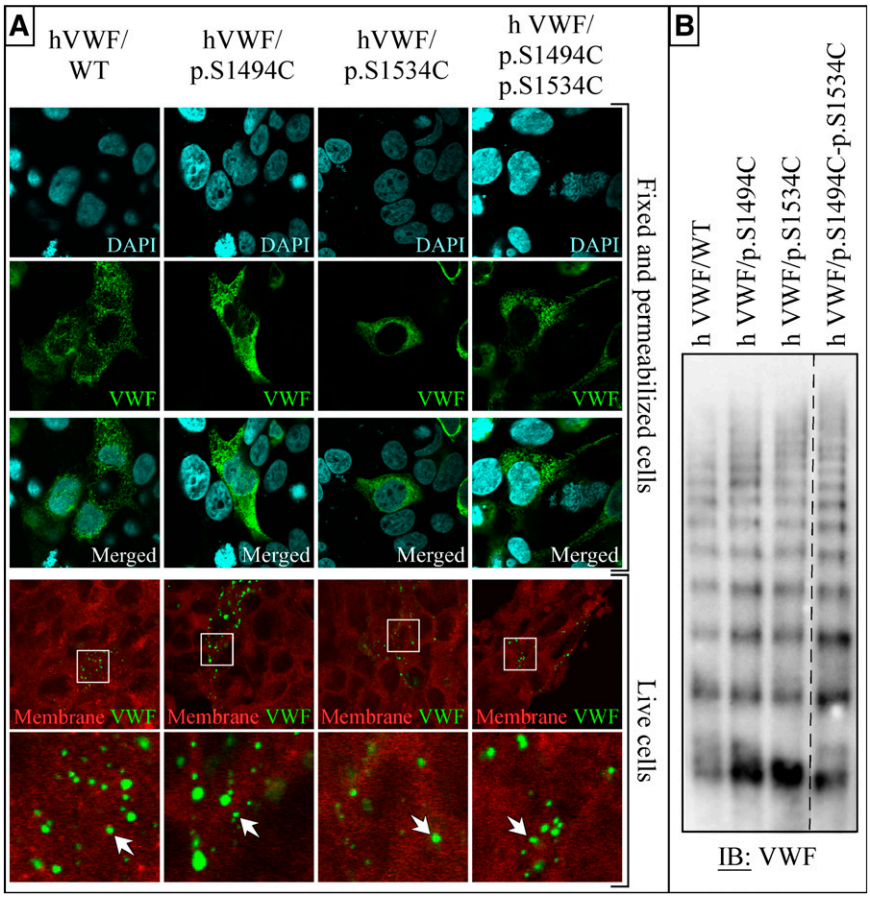

Figure 1. Expression of VWF in HA-HRH1 HEK293T. (A) Representative staining of transiently transfected cells with or without fixation and permeabilization. Fixed cells were costained for DNA (4′,6 diamidino-2-phenylindole) and VWF (Alexa-Fluor 488); a large number of Weibel-Palade body-like structures can be observed throughout the cytoplasm of both WT and all 4 mutant VWF-transfected cells. (The data are representative of 3 independent experiments in which each construct was transfected in 3 × 8-well slides. A minimum of 10 microscopic fields per well were photographed for a total of >240 fields analyzed per construct.) Live histamine-treated cells were costained with the plasma membrane marker CellMask DeepRed (red) and anti-VWF antibody (Alexa-Fluor 488). VWF-rich domains can be seen on the surface of some of the cells (magnified fields are shown in the right column). No differences were observed between WT and mutant VWF-expressing cells. (The data are representative of 3 independent experiments in which each construct was transfected in 3 × 8-well slides. A minimum of 5 microscopic fields per well were photographed for a total of >120 fields analyzed per construct.) Wide field images were captured at an original magnification of ×63 (1.4 aperture) and high-magnification images at ×100 (1.4 aperture). All images were captured on a LSM 510 Meta confocal microscope. Capture of live samples was performed at 37°C; all other samples were photographed at room temperature. Fixed samples were mounted in Vectashield mounting medium (Vector Laboratories, Burlingame, CA). All images were captured and processed with the LSM 510 software. (B) Samples taken from cells transfected with VWF WT, VWF/p.S1494C, VWF/p.S1534C, and VWF/p.S1494-p.S1534C were run on a 2% agarose 0.1% SDS gel. After transfer, membranes were analyzed for VWF expression. The dashed line indicates that part of the immunoblot is cropped to exclude irrelevant samples. All constructs expressed as multimerized proteins when expressed in HEK293T cells (n = 2).

of the protein, thereby promoting platelet binding. However, mutant VWF/p.S1494C-p.S1534C proved similar as VWF/WT in binding to nanobody AU/VWFa-11 (activation factor-ratio mutant/WT 0.84 ± 0.33; n = 5), whereas for the positive control type 2B mutant VWF/p.R1306Q, this ratio was 18 ± 8 (n = 3; data not shown). Thus, the higher platelet-binding potential of the double mutant does not originate from an intrinsically more active conformation than VWF/WT, but rather may be due to an increased sensitivity to shear stress-induced exposure of the A1 domain.

Cysteines 1494 and 1534 form a disulfide bridge that renders VWF A2 resistant to proteolysis in vitro

We hypothesized that substituting cysteine residues to Ser1494 and Ser1534 would result in the formation of a novel disulfide bond within the A2 domain of VWF (which already contains a vicinal disulfide bond at C1669-C1670). Within the A2 domain, the β1-strand interfaces directly with the cleavage site on the β4-strand.[18] In theory, this bond would prevent the unfolding of the β1-α1 loop and prevent proteases from accessing the cleavage site (Figure 3A). To demonstrate that such a disulfide bond had formed, recombinant A2/WT and A2/p.S1494C-p.S1534C proteins were generated and subjected to sulfhydryl group labeling by Oregon green 488-maleimide after reduction by β-mercaptoethanol. As expected, untreated A2/WT and A2/p.S1494C-p.S1534C showed no detectable Oregon green 488-maleimide labeling, thus confirming the absence of free thiol groups in these proteins. Reduced A2/WT was found to incorporate a significant amount of Oregon green 488-maleimide, which can only be attributed to newly formed sulfhydryl groups on cysteines 1669 and 1670. Reduced A2/p.S1494C-S1534C was found to incorporate ~2 times as much Oregon green 488-maleimide as A2/WT (mean ± standard error [SE]: 0.512 ± 0.077 and 1.23 ± 0.351, respectively), thus confirming that twice as many sulfhydryl groups had become exposed (Figure 3B). These results unequivocally show that the sulfhydryl goups on all 4 cysteine residues in A2/p.S1494C-p.S1534C are oxidized and form 2 disulfide bridges.

To demonstrate that the newly formed C1494-C1534 disulfide bond confers protease resistance to the host domain, recombinant A2/WT and A2/p.S1494C-p.S1534C proteins were subjected to plasma protease treatment in the absence or presence of a reducing agent. Although no difference was observed in the rate of proteolysis of both native and reduced A2/WT, cleavage of A2/p.S1494C-p.S1534C could only be achieved through β-mercaptoethanol treatment (Figure 3C). Similarly, although almost complete degradation of A2/WT could be achieved after overnight trypsin treatment, only limited A2/p.S1494C-p.S1534C proteolysis could be observed under the same condition (P = .0000382; Figure 3D). Taken together, these findings show that a novel disulfide bond formed between Cys1494 and Cys1534 and that it renders the A2 domain of VWF resistant to proteolysis by plasma proteases and trypsin as well.

Hydrodynamic injection of pLIVE-m VWF/p.S1494C-p.A1534C constructs causes mice to develop thrombocytopenia and schistocytes

For in vivo analysis, we subsequently focused on the VWF/p.S1494C-p.S1534C double mutant (mVWF/p.S1494C-A1534C for murine VWF), as the single mutations display behavior similar to

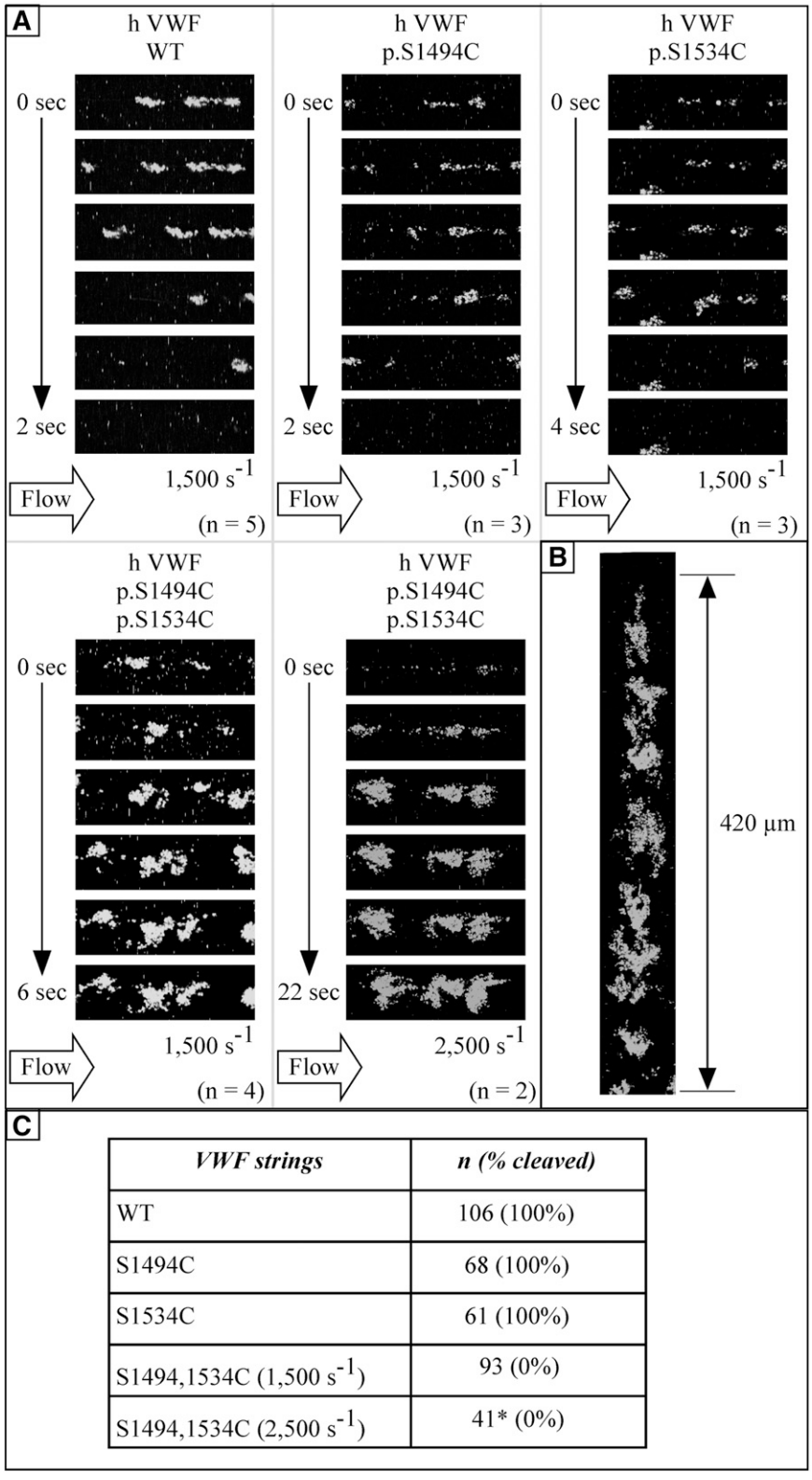

VWF strings	*n (% cleaved)*
WT	106 (100%)
S1494C	68 (100%)
S1534C	61 (100%)
S1494,1534C (1,500 s^{-1})	93 (0%)
S1494,1534C (2,500 s^{-1})	41* (0%)

Figure 2. Human VWF p.S1494C-p.S1534C is resilient to proteolysis under flow. pCMV6-XL5-VWF-transfected HA-HRH1 HEK293T cells are grown inside poly-L-lysine-coated flow chambers and exposed to mepacrine-labeled whole blood at flow rates of 1500 and 2500 s^{-1}. (A) Corresponding movies can be found in the supplemental Methods. VWF/WT, VWF/p.S1494C, or VWF/p.S1534C strings are systematically severed when exposed to whole blood at shear rates of 1500 s^{-1} or above. VWF strings containing the p.S1494C-p.S1534C double mutation are, however, utterly resistant to proteolysis, even at higher shear rates (2500 s^{-1}). As a result, VWF/p.S1494C-p.S1534C strings are able to support the formation of massive thrombi by capturing circulating blood platelets (n refers to the number of individual experiments performed for each construct). (B) VWF/p.S1494C-p.S1534C strings vary in length (from ~100 μm to >1 mm). Reconstruction of a 420-μm string captured over multiple photographic fields is presented as an example. (C) The table summarizes the total number of VWF strings analyzed (n) for each construct. VWF/WT, VWF/p.S1494C, and VWF/p.S1534C strings were found to be systematically cleaved on exposure to plasma proteases. None of the 93 VWF/p.S1494C-p.S1534C strings analyzed at 1500 s^{-1} were cleaved after up to 5-minute exposure to whole blood. Similarly, no cleavage of VWF/p.S1494C-p.S1534C strings was observed at 2500 s^{-1}; however, of the 44 strings observed, 3 could not be included in the analysis because of the detachment of the cells they were tethered to (*). Original magnification, ×63 (aperture 1.4). All videos were captured on a LSM 510 Meta confocal microscope at 37°C and processed with the LSM 510 software.

VWF/WT in the in vitro assays. VWF/WT and the double mutant were expressed via hydrodynamic gene transfer in VWF-deficient mice. Blood samples were collected 4 and 7 days after injection and analyzed for VWF antigen, platelet counts, and multimeric pattern.

In accordance with our previous in vivo studies involving hydrodynamic injection-mediated expression of VWF, mice were included expressing VWF antigen levels between 300% and 1000%.[16,19,20] At both 4 and 7 days after injection, antigen levels were similar for mVWF/WT and mVWF/p.S1494C-p.A1534C. At day 4, antigen levels were 688 ± 208% (mean ± standard deviation [SD]; n = 6) and 697 ± 302% (n = 7; unpaired Student *t* test: $P > .05$) for mVWF/WT and mVWF/p.S1494C-p.A1534C, respectively. At

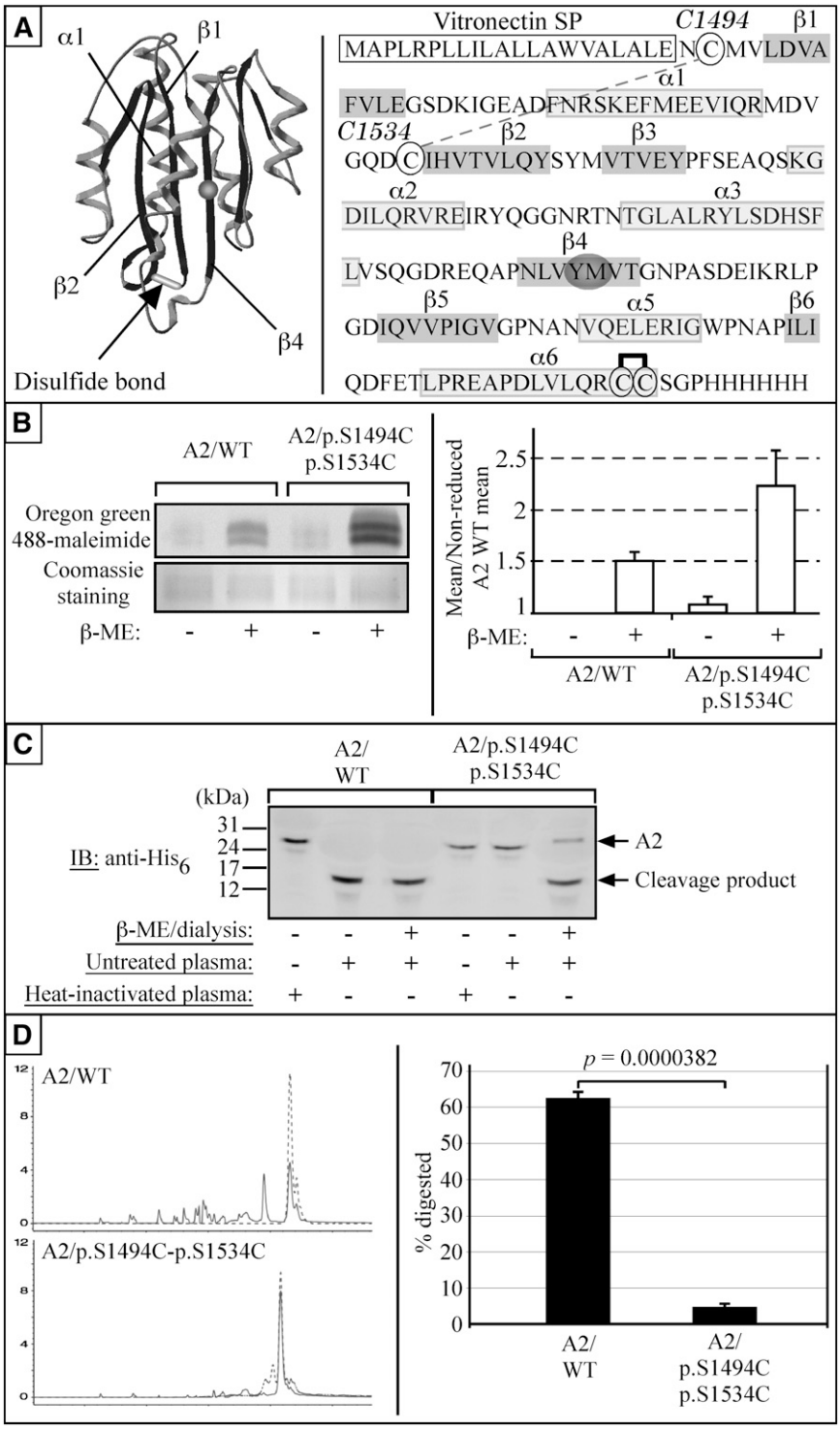

Figure 3. S1494C and S1534C form a disulfide bond that renders the A2 domain of VWF resistant to proteolysis by plasma proteases and trypsin. (A) Cysteine 1494 and 1534 are projected to form a disulfide bond linking the amino-terminal ends of the β1 and β2 strands, thereby making the unfolding of the β1-α1-β2 subdomain more difficult. The recombinant A2 domain used in our studies is flanked by the human vitronectin signal peptide (Vn_{SP}) and a carboxy-terminal His_6 tag. Cysteine 1494 and 1534 are circled, as well as cysteine 1669 and 1670 (engaged in a vicinal disulfide bridge). (B) In the absence of reducing agent, neither A2/WT nor A2/p.S1494C-S1534C displays any Oregon green 488-maleimide labeling. However, on β-mercaptoethanol (β-ME) treatment and resulting sulfhydryl moieties exposure, both A2/WT and A2/p.S1494C-S1534C show Oregon-green 488-maleimide incorporation (n = 3). To quantify the difference in Oregon green 488-maleimide incorporation from one sample to the other, the mean immunofluorescence intensity of each bands was quantified with NIH ImageJ 1.41 software. The measured means for all 3 gels were then averaged and expressed as a fraction of the nonreduced A2/WT mean. Error bars indicate SE. The difference in signal (~2) accounts for the number of disulfide bonds having been reduced in the 2 proteins (1 such bond in A2/WT and 2 for A2/p.S1494C-S1534C). The black and white image of the fluorescent gel was obtained through Photoshop gray-scale mode adjustment and tone inversion of the original scan. The gel was subsequently stained with Coomassie blue as a loading control. (C) A2/WT and A2/p.S1494C-p.S1534C were incubated with platelet-poor plasma overnight at 37°C with or without prior β-ME and analyzed by SDS-polyacrylamide gel electrophoresis on a 17% acrylamide gel. Although A2/WT is cleaved under both conditions, A2/p.S1494C-p.S1534C is only cleaved after β-ME treatment (n = 3). (D) Similarly, A2/p.S1494C-p.S1534C shows stronger resistance to trypsin digestion than A2/WT. Statistical analysis shows that 62.06 ± 1.67% (mean ± SE) of A2/WT is proteolyzed by trypsin, whereas only 4.66 ± 0.84% (mean ±SE) of A2/p.S1494C-p.S1534C is degraded under the same condition. The probability associated with a Student *t* test is 3.82×10^{-5} (n = 7).

day 7, antigen levels were 553 ± 234% (n = 6) and 660 ± 212% (n = 7; $P > .05$) for mVWF/WT and mVWF/p.S1494C-p.A1534C, respectively.

Multimer analysis revealed that for mVWF/WT, the full range of multimers was present both at day 4 and day 7 (Figure 4A). A more extended range of multimers was present for mice expressing mutant mVWF/p.S1494C-p.A1534C at both day 4 and day 7. Interestingly, the ratio high molecular weight (11-20 bands)/low molecular weight (1-5 bands) multimers was increased for mutant VWF (0.09 ± 0.04) compared with VWF/WT (0.03 ± 0.02): bands representing dimers and tetramers were more intense for VWF/WT compared with mutant VWF. This increased ratio seems compatible with the presence of VWF that is resistant against proteolytic degradation.

Interestingly, Coulter platelet counts were significantly different between mVWF/WT and mVWF/p.S1494C-p.A1534C at both day 4 and day 7 after injection (Figure 4B). At day 4, platelet counts were 715 ± 107 (mean ± SD; n = 6) and 373 ± 339 (n = 7; $P = .0397$) for mVWF/WT and mVWF/p.S1494C-p.A1534C, respectively. At day

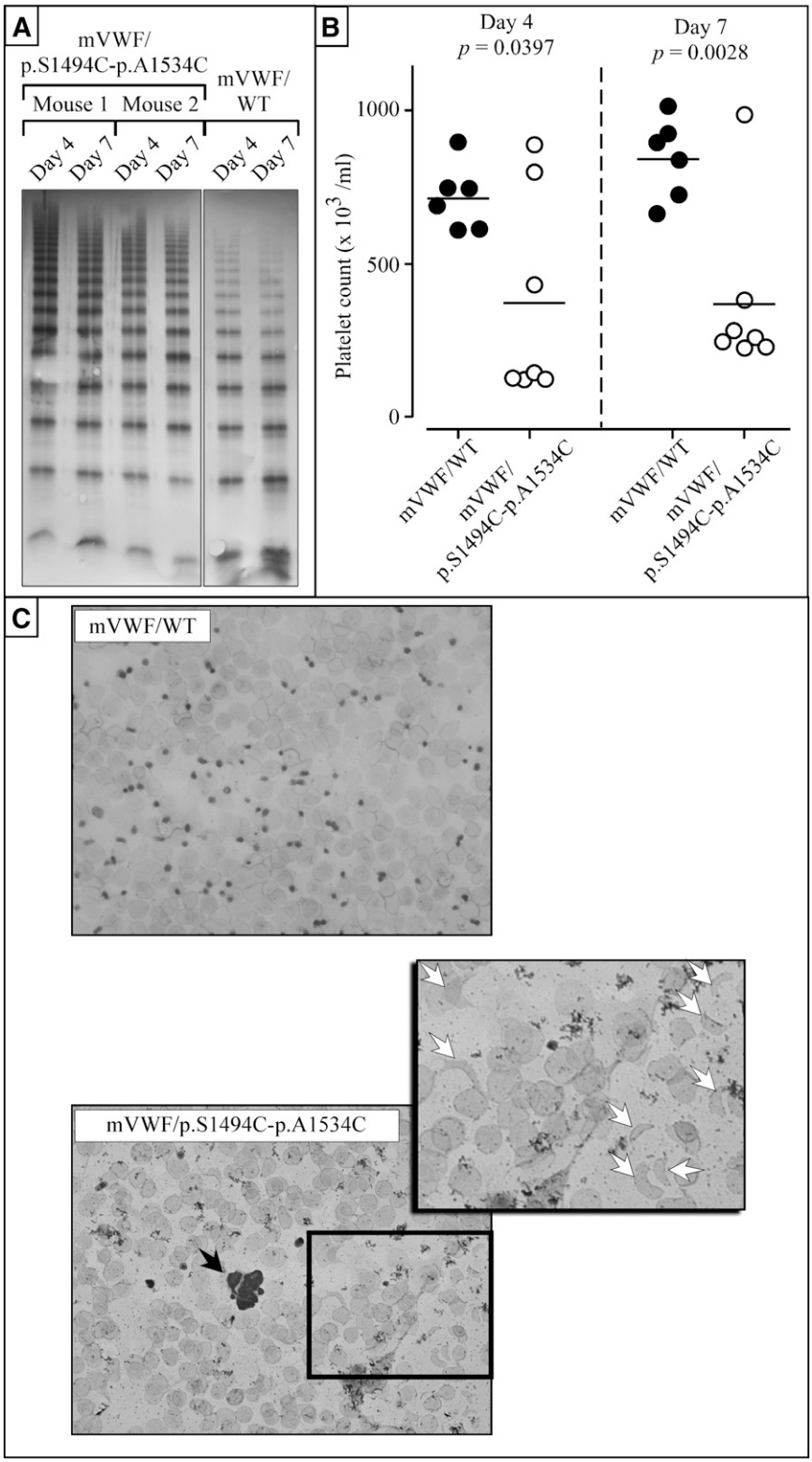

Figure 4. Mice expressing murine VWF/p.S1494C-p.A1534C are thrombocytopenic and present with schistocytes. Every mouse used in this study is $VWF^{-/-}$. (A) Multimer analysis of plasma taken from mice expressing mVWF/p.S1494C-p.A1534C (mice 1 and 2) or mVWF/WT at day 4 and day 7 after hydrodynamic injection using 2% SDS-agarose gel electrophoresis. Gels were loaded with 0.1 μg antigen per lane. All multimers originate from the same multimer gel. (B) Coulter platelet counts and plasma VWF antigen ratio were measured at days 4 and 7 after injection. Only mice with VWF antigen levels within the 300% to 1000% normal range were included in this study. Significant differences were found in platelet counts between mVWF/WT-expressing mice and mVWF/p.S1494C-p.A1534C-expressing mice. Although mVWF/WT mice have normal platelet counts at both time points, 5 of 7 mVWF/p.S1494C-p.A1534C mice were found to be thrombocytopenic at day 4 and 6 of 7 by day 7. (C) Blood smears were prepared with heparinized blood from mice injected with normal and mutant pLIVE-mVWF constructs and subjected to GIEMSA staining. Although mice expressing mVWF/WT do not present with any anomalies, mice expressing mVWF/p.S1494C-p.A1534C present with occasional platelet aggregates (black arrow), schistocytes (white arrows), and fewer platelets and erythrocytes. For each mouse, 2 blood smears were prepared, and 5 mice were analyzed for each construct. Wide field images were captured at an original magnification of ×63 (1.4 aperture) and high-magnification images at ×100 (1.4 aperture). All images were captured on a LSM 510 Meta confocal microscope at room temperature. All images were captured and processed with the LSM 510 software.

7, platelet counts were 841 ± 131 (n = 6) and 369 ± 277 (n = 7; 0.0028) for mVWF/WT and mVWF/p.S1494C-p.A1534C, respectively. At both time points, none of the mVWF/WT-expressing mice displayed platelet counts below 600, whereas 5 of 7 (Fisher's exact test: $P = .02$) and 6 of 7 ($P = .005$) mice for mVWF/p.S1494C-p.A1534C displayed platelet counts below 450 at days 4 and 7, respectively (Figure 4B).

These findings show that platelet depletion keeps on occurring in the days that follow the early onset of thrombocytopenia. Giemsa staining of blood smears taken from both mouse groups confirmed that animals expressing VWF/WT have normal platelet and red cell numbers (Figure 4C). Blood smears from mice expressing the double mutant, on the other hand, reveal multiple anomalies. These blood films have fewer red cells, very few platelets, and present with

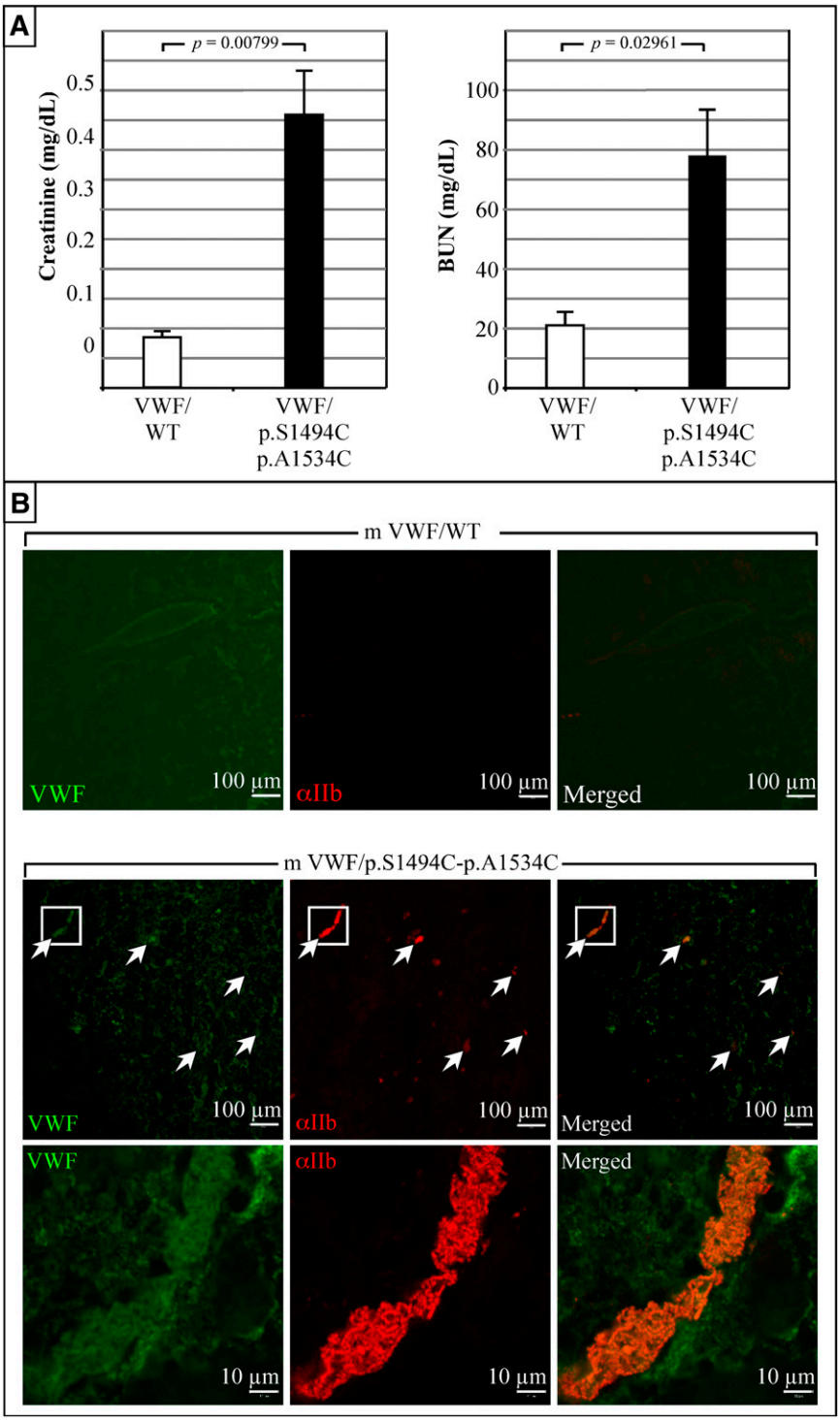

Figure 5. Expression of mVWF/p.S1494C-p.A1534C in mice is associated with abnormal renal functions. (A) Blood creatinine and BUN levels were measured at day 4 after injection (in duplicates and on 5 mice for each construct). Elevated creatinine and BUN levels in pLIVE-mVWF/p.S1494C-p.A1534C-injected mice show that these animals suffer from abnormal kidney functions. Values plotted are the mean ± SE. Student *t* test was performed on both sets of data. (B) Histological analysis of kidneys taken from animals at day 4 after injection. These photographs are representative of tissue staining performed on 5 animals per construct. No platelet staining was seen in the kidneys of mice expressing mVWF/WT. Conversely, mVWF/p.S1494C-p.A1534C-expressing mice present with numerous platelet clots in the kidney vasculature. Those clots generally colocalize with large VWF deposits. High magnification (×100) of the longitudinal view of 1 such vessel shows nearly complete occlusion by VWF-rich thrombi. Wide field images were captured at an original magnification of ×63 (1.4 aperture) and high-magnification images at ×100 (1.4 aperture). All images were captured on a LSM 510 Meta confocal microscope at room temperature. Samples were mounted in Vectashield mounting medium (Vector Laboratories). All images were captured and processed with the LSM 510 software.

occasional platelet microaggregates and schistocytes (Figure 4C). Interestingly, the extent of the thrombocytopenia seen in these animals was found to vary with the nature of the assay used to assess platelet number, with size-based particle counting of plasma samples (Figure 4B) yielding higher platelet counts than GIEMSA-stained smeared blood samples (Figure 4C). This discrepancy is probably due to the presence of schistocytes in the blood of these animals; red cell fragments being indistinguishable from platelets in the Coulter particle counter, they may cause platelet numbers to be overestimated.

Overall, these studies show that expression of mVWF/p.S1494C-p.A1534C in mice is associated with a range of blood disorders that are considered hallmarks of TTP in humans.

mVWF/p.S1494C-p.A1534C mice present with renal dysfunction

At day 4 after injection, blood samples were collected from mice and analyzed for creatinine and blood urea nitrogen (BUN) contents (Figure 5A). Mice expressing mVWF/WT have normal creatinine and BUN levels (mean = 0.084 ± 0.008 mg/dL; n = 5 and

mean = 21 ± 2 mg/dL; n = 5, respectively). Conversely, mVWF/p.S1494C-p.A1534C mice have five- to sixfold increased creatinine (mean = 0.45 ± 0.07 mg/dL; n = 5) and three- to fourfold increased BUN levels (mean = 77. ± 15 mg/dL; n = 5), which are indicative of impaired kidney function (Figure 5A). To further investigate these findings, organs were harvested from these animals at day 4 after injection for histological analysis. Although control mice were asymptomatic, kidneys from mice expressing mVWF/p.S1494C-p.A1534C presented with widespread bruising (supplemental Figure 1A). Immunostaining of frozen sections taken from these animals revealed the presence of numerous VWF-rich platelet aggregates throughout the kidney vasculature (Figure 5B). The apparent high VWF content of these thrombi suggests that circulating thrombogenic VWF is indeed responsible for the capture of platelets and the accumulation of thrombi in renal blood vessels. Although histological analysis of brain, lung, and hepatic tissues did not reveal any significant difference between control and double-mutant mice (data not shown), severe liver bruising was seen in most double VWF mutant mice (supplemental Figure 1B). Last, half of mVWF/p.S1494C-p.A1534C mice suffered from splenomegaly (supplemental Figure 1C).

Discussion

The aim of this study was the creation of a mouse model that mimics the clinical features of TTP. To achieve that goal, VWF mutants exhibiting various cysteine substitutions were created. Our hypothesis was that if some of the mutants were able to form disulfide bonds within the A2 domain, they would become resilient to deformation by flow forces and proteolysis by plasma proteases. A novel cell-based flow model was created with the intent of testing these VWF mutants in a context as physiologically relevant as possible. As reported elsewhere,[21] HEK293T cells have the ability to synthetize, package, and secrete VWF in the form of long multimers (strings). In an attempt to further improve on that model, we created the HA-HRH1 HEK293T cell line that stably expresses the human histamine receptor 1. Histamine treatment of these cells was found to result in cell surface exposure of secreted VWF multimers in structures resembling the VWF dots seen in endothelial cells.[17] To trigger the unfurling of these VWF multimers, a novel in vitro cell flow system was designed. In this model, HA-HRH1 HEK293T cells are grown in poly-L-lysine-coated flow chambers and subjected to high shear flow forces 2 to 3 days after transfection. Flow analysis is performed 2 times. Cells are first exposed to a plasma-free blood cell suspension to allow the detection of UL-VWF multimers in the flow chamber in the absence of protease. Once platelet-decorated UL-VWF multimers have been identified, whole blood is injected into the flow chamber to assess the thrombogenic potential and protease susceptibility of each VWF mutant. Exposure of HEK293T cells to high shear rates revealed that cell surface-tethered VWF strings can support the formation of large platelet aggregates. In agreement with previous work by Nishio et al that showed that binding of platelet receptor GpIbα to the A1 domain of VWF facilitates A2 cleavage by ADAMTS13,[13] severance of VWF/WT, VWF/p.S1494C, and VWF/p.S1534C strings was only seen after platelet binding had occurred. VWF mutants bearing the p.S1494C-p.S1534C double substitution were found to be resilient to cleavage by plasma proteases under flow and were highly thrombogenic.

Analysis of recombinant A2 domains confirmed that the p.S1494C-p.S1534C mutation was conducive to the formation of a novel internal disulfide bond and that chemical reduction of this bond was required for A2/p.S1494C-p.S1534C cleavage. A Cys1494 to Cys1534 covalent bond would, in theory, prevent the dissociation of the β1 and α1 A2 subdomains. Because the cleavage site for ADAMTS13 is located on the β4-strand,[22] a structurally constrained β1 would, in theory, prevent access to adjacent β4 binding sites (Figure 3A). Whether these mutations prevent protease recruitment to VWF all together or cause a misalignment of the enzymes catalytic domains with important A2 residues remains to be determined. In the case of ADAMTS13, binding sites have been identified inside and outside the A2 domain.[23] One such site includes Leu1603, located on the β4-strand. Mutation of Leu1603 was reported to block ADAMTS13 cleavage of VWF but not their association.[24] It is therefore conceivable that a β4-strand-proximal steric hindrance due to the Cys1494-Cys1534 bond would primarily affect cleavage rather than binding of the protease. Another possible mechanism through which the p.S1494C-p.S1534C double mutation may confer cleavage resistance to VWF might involve the A2 Ca^{2+} binding site identified by Zhou et al in their alternate A2 domain crystal structure. The resolved structure published by this group shows that 2 of the 4 residues forming this Ca^{2+} binding site are located on the β1 and β4 strands of A2.[25] It is therefore conceivable that a structurally constrained β1 would reinforce the stabilizing action Ca^{2+} has on the A2 domain, thereby preventing its unfolding under shear. Follow-up studies will have to be undertaken to further address these issues.

In acute acquired TTP patients, symptoms are triggered by widespread thrombosis due to the presence of large uncleaved VWF multimers in the circulation. As a result, patients initially present with thrombocytopenia, VWF-rich platelet aggregates, and schistocytes (due to the mechanical fragmentation of erythrocytes in partially occluded vessels). As the disease progresses, they may present with enlarged spleens (splenomegaly), neurological impairment (~65% of patients), kidney dysfunction, and heart failure. Vectors encoding mVWF/WT and mVWF/p.S1494C-p.A1534C were injected into mice by hydrodynamic injection to assess their ability to elicit TTP-like symptoms in VWF-null mice. Within 4 days of the injection, WT and mutant VWF multimers could be detected in the plasma of these mice at levels comparable to normal C57Bl/6 VWF plasma levels and up to 10 times higher.

The presence of small-size VWF multimers in the plasma of mVWF/p.S1494C-p.A1534C-expressing animals suggests that proteases other than ADAMTS13 can take on the processing of VWF, an observation that echoes previous findings by other groups.[6,7,26] A number of candidate proteases capable of cleaving VWF have been identified, such as cytotoxic lymphocyte T cell- and natural killer cell-secreted granzyme B and M,[27,28] leukocyte-derived cathepsin G, elastase, matrix metalloproteinase 9, and plasmin.[22,29] Although elastase, matrix metalloproteinase, and cathepsin G have been shown to have either identical or proximal cleavage sites to ADAMTS13, plasmin and granzyme B and M appear to cleave VWF at more distant sites. The relevance of alternative proteases in regulating VWF multimer size has recently been demonstrated in an elegant study by Tersteeg et al,[30] revealing that plasmin can function as a backup system in the absence of ADAMTS13. For the present study, we have not yet tested other proteases with regard to the ADAMTS13-resistant double mutant. However, given the notion that leukocyte-derived proteases cleave VWF within the similar A2 domain region as ADAMTS13, we anticipate that the double mutant will be resistant against proteolysis by these proteases as well. This issue will be subject of investigation in future studies by our group.

Interestingly, mVWF/p.S1494C-p.A1534C was found to preferentially form higher-molecular-weight multimers, whereas lower-molecular-size multimers were observed for mVWF/WT. Even at day 7, mice expressing mutant mVWF did have HMW multimers, despite the presence of strongly reduced platelet counts ($<300 \times 10^3/\mu L$). Previously, it has been reported that there is a frequent loss of HMW multimers with acute TTP,[31] a phenomenon that is not reproduced in our mouse model. One explanation for this apparent discordance could be that the amount of HMW-VWF that is consumed into VWF-platelet aggregates is relatively small compared with the amount of circulating VWF and hence escapes detection via multimeric analysis.

Unlike UL-VWF multimers which are partially in an active, platelet-binding conformation, mVWF/p.S1494C-p.A1534C multimers proved similar to VWF/WT in binding to nanobody AU-VWFa-11, which specifically detects the active conformation present in UL-VWF or VWD-type 2B.[12] This indicates that the double mutant lacks the intrinsic potential to spontaneously interact with platelets. To explain its higher platelet binding potential in the circulation and in the in vitro perfusion assays, we can but speculate at this moment. It is known that the A2 domain plays a role in the exposure of the platelet-binding A1 domain.[32] In globular VWF, the A2 domain is in close proximity to the A1 domain, interfering with platelet access to the A1 domain. Under elevated shear stress conditions, the A2 moves away from the A1 domain, allowing platelet binding. We anticipate that the increased disulfide bridge-induced rigidity of the A2 domain promotes its moving away from the A1 domain even under low shear stress conditions. This increased platelet binding potential cannot be counteracted via ADAMTS13-mediated proteolysis. Apparently, the combination of both ADAMTS13 resistance and more shear stress-sensitive exposure of the platelet-binding site contribute to the thrombogenicity of the mutant. In any case, mice expressing murine VWF/p.S1494C-p.A1534C were found to develop symptoms very similar to the ones seen in TTP patients: presence of VWF-rich platelet aggregates in the vasculature, thrombocytopenia, red cell fragmentation, renopathy, and occasional splenomegaly. Neurological and cardiac impairments were not assessed in those animals but may be occurring as well.

In conclusion, we developed a novel model of microangiopathic disease that accurately mimics TTP symptoms and that can be used for various further investigations. First, it provides an alternative approach to existing chemically, mechanically, or heat-induced in vivo thrombosis models,[15,33,34] allowing it to study the role of continuous platelet aggregation in the context of thrombosis and hemostasis. Furthermore, this system is based on interactions between VWF and its platelet receptor GpIb and could therefore be used as an in vivo model to study molecular events responsible for the transition of rolling platelets into fully active, firmly adherent platelets. Also from the perspective of our understanding of thrombotic microangiopathies (TMAs), our model could be of relevance. TMA is generally defined as a combination of microangiopathic hemolytic anemia, thrombocytopenia, and microvascular thrombosis. The initial therapy for all TMAs is plasma exchange, an expensive, cumbersome procedure with such potential side effects as infection, cardiac arrest, venous thrombosis, or hypotension. Although we realize that our model is ill-suited for the study of ADAMTS13-based TTP therapies, it provides several other advantages. It could be useful for preclinical testing of therapies capable of disrupting VWF-platelet interactions, conceptually similar to ALX0081 and ARC15105 that have been tested in a clinical setting for the treatment and prevention of acute and chronic TMA. Finally, our model provides a platform to investigate effects secondary to the occlusion of vessels by VWF/platelet aggregates, in particular, organ damage, neuronal aberrations, and schistocyte formation. Thus, our model could be helpful in further delineating thrombotic processes and their secondary effects, as well as in the development of novel therapeutic strategies in the treatment of TMA.

Acknowledgments

The authors thank Paulette Legendre for conducting the mouse plasma multimer analysis.

This work was supported by funds from the Japanese Society for the Promotion of Science and funds from the Ministry of Education, Sports, Science and Technology of Japan.

Authorship

Contribution: Y.M., C.C., N.W., and S.C. designed and performed experiments and analyzed data; S.K. and A.K. provided technical assistance; O.D.C., R.L., and C.V.D. designed experiments and contributed essential reagents to the study; P.J.L. designed experiments, analyzed data, and contributed to the redaction of manuscript; N.P. designed and performed experiments, analyzed data, and wrote the manuscript; and all authors were involved in reviewing the manuscript.

Conflict-of-interest disclosure: The authors declare no competing financial interests.

Correspondence: Nicolas Prévost, Kyoto University, Career-Path Unit for Young Life Scientists, Sakyo-ku, Yoshida, Konoe-cho, 606-8501 Kyoto, Japan; e-mail: nprevost@cp.kyoto-u.ac.jp.

References

1. Furlan M, Robles R, Lämmle B. Partial purification and characterization of a protease from human plasma cleaving von Willebrand factor to fragments produced by in vivo proteolysis. *Blood.* 1996;87(10):4223-4234.
2. Levy GG, Nichols WC, Lian EC, et al. Mutations in a member of the ADAMTS gene family cause thrombotic thrombocytopenic purpura. *Nature.* 2001;413(6855):488-494.
3. Sporn LA, Marder VJ, Wagner DD. Inducible secretion of large, biologically potent von Willebrand factor multimers. *Cell.* 1986;46(2):185-190.
4. Moake JL, Rudy CK, Troll JH, et al. Unusually large plasma factor VIII:von Willebrand factor multimers in chronic relapsing thrombotic thrombocytopenic purpura. *N Engl J Med.* 1982;307(23):1432-1435.
5. Moake JL. Thrombotic microangiopathies. *N Engl J Med.* 2002;347(8):589-600.
6. Vanhoorelbeke K, De Meyer SF. Animal models for thrombotic thrombocytopenic purpura. *J Thromb Haemost.* 2013;11(Suppl 1):2-10.
7. Banno F, Kokame K, Okuda T, et al. Complete deficiency in ADAMTS13 is prothrombotic, but it alone is not sufficient to cause thrombotic thrombocytopenic purpura. *Blood.* 2006;107(8):3161-3166.
8. Motto DG, Chauhan AK, Zhu G, et al. Shigatoxin triggers thrombotic thrombocytopenic purpura in genetically susceptible ADAMTS13-deficient mice. *J Clin Invest.* 2005;115(10):2752-2761.
9. Zhang X, Halvorsen K, Zhang CZ, Wong WP, Springer TA. Mechanoenzymatic cleavage of the ultralarge vascular protein von Willebrand factor. *Science.* 2009;324(5932):1330-1334.
10. Wu T, Lin J, Cruz MA, Dong JF, Zhu C. Force-induced cleavage of single VWFA1A2A3 tridomains by ADAMTS-13. *Blood.* 2010;115(2):370-378.

11. Lenting PJ, Westein E, Terraube V, et al. An experimental model to study the in vivo survival of von Willebrand factor. Basic aspects and application to the R1205H mutation. *J Biol Chem.* 2004;279(13):12102-12109.
12. Hulstein JJ, de Groot PG, Silence K, Veyradier A, Fijnheer R, Lenting PJ. A novel nanobody that detects the gain-of-function phenotype of von Willebrand factor in ADAMTS13 deficiency and von Willebrand disease type 2B. *Blood.* 2005; 106(9):3035-3042.
13. Nishio K, Anderson PJ, Zheng XL, Sadler JE. Binding of platelet glycoprotein Ibalpha to von Willebrand factor domain A1 stimulates the cleavage of the adjacent domain A2 by ADAMTS13. *Proc Natl Acad Sci U S A.* 2004; 101(29):10578-10583.
14. Savage B, Sixma JJ, Ruggeri ZM. Functional self-association of von Willebrand factor during platelet adhesion under flow. *Proc Natl Acad Sci USA.* 2002;99(1):425-430.
15. Marx I, Christophe OD, Lenting PJ, et al. Altered thrombus formation in von Willebrand factor-deficient mice expressing von Willebrand factor variants with defective binding to collagen or GPIIbIIIa. *Blood.* 2008;112(3):603-609.
16. Denis C, Methia N, Frenette PS, et al. A mouse model of severe von Willebrand disease: defects in hemostasis and thrombosis. *Proc Natl Acad Sci USA.* 1998;95(16):9524-9529.
17. Valentijn KM, van Driel LF, Mourik MJ, et al. Multigranular exocytosis of Weibel-Palade bodies in vascular endothelial cells. *Blood.* 2010;116(10): 1807-1816.
18. Zhang Q, Zhou YF, Zhang CZ, Zhang X, Lu C, Springer TA. Structural specializations of A2, a force-sensing domain in the ultralarge vascular protein von Willebrand factor. *Proc Natl Acad Sci USA.* 2009;106(23):9226-9231.
19. Rayes J, Hollestelle MJ, Legendre P, et al. Mutation and ADAMTS13-dependent modulation of disease severity in a mouse model for von Willebrand disease type 2B. *Blood.* 2010;115(23): 4870-4877.
20. Casari C, Du V, Wu YP, et al. Accelerated uptake of VWF/platelet complexes in macrophages contributes to VWD type 2B-associated thrombocytopenia. *Blood.* 2013;122(16): 2893-2902.
21. Wang JW, Valentijn JA, Valentijn KM, et al. Formation of platelet-binding von Willebrand factor strings on non-endothelial cells. *J Thromb Haemost.* 2012;10(10):2168-2178.
22. Raife TJ, Cao W, Atkinson BS, et al. Leukocyte proteases cleave von Willebrand factor at or near the ADAMTS13 cleavage site. *Blood.* 2009; 114(8):1666-1674.
23. Crawley JT, de Groot R, Xiang Y, Luken BM, Lane DA. Unraveling the scissile bond: how ADAMTS13 recognizes and cleaves von Willebrand factor. *Blood.* 2011;118(12): 3212-3221.
24. Xiang Y, de Groot R, Crawley JT, Lane DA. Mechanism of von Willebrand factor scissile bond cleavage by a disintegrin and metalloproteinase with a thrombospondin type 1 motif, member 13 (ADAMTS13). *Proc Natl Acad Sci USA.* 2011; 108(28):11602-11607.
25. Zhou M, Dong X, Baldauf C, et al. A novel calcium-binding site of von Willebrand factor A2 domain regulates its cleavage by ADAMTS13. *Blood.* 2011;117(17):4623-4631.
26. De Meyer SF, Budde U, Deckmyn H, Vanhoorelbeke K. In vivo von Willebrand factor size heterogeneity in spite of the clinical deficiency of ADAMTS-13. *J Thromb Haemost.* 2011;9(12):2506-2508.
27. Hollestelle MJ, Lai KW, van Deuren M, et al. Cleavage of von Willebrand factor by granzyme M destroys its factor VIII binding capacity. *PLoS ONE.* 2011;6(9):e24216.
28. De Ceunynck K, De Meyer SF, Vanhoorelbeke K. Unwinding the von Willebrand factor strings puzzle. *Blood.* 2013;121(2):270-277.
29. Berkowitz SD, Dent J, Roberts J, et al. Epitope mapping of the von Willebrand factor subunit distinguishes fragments present in normal and type IIA von Willebrand disease from those generated by plasmin. *J Clin Invest.* 1987;79(2): 524-531.
30. Tersteeg C, de Maat S, De Meyer SF, et al. Plasmin Cleavage of von Willebrand Factor as an Emergency Bypass for ADAMTS13 Deficiency in Thrombotic Microangiopathy. *Circulation.* 2014; 129(12):1320-1331.
31. Lotta LA, Lombardi R, Mariani M, et al. Platelet reactive conformation and multimeric pattern of von Willebrand factor in acquired thrombotic thrombocytopenic purpura during acute disease and remission. *J Thromb Haemost.* 2011;9(9): 1744-1751.
32. Martin C, Morales LD, Cruz MA. Purified A2 domain of von Willebrand factor binds to the active conformation of von Willebrand factor and blocks the interaction with platelet glycoprotein Ibalpha. *J Thromb Haemost.* 2007;5(7): 1363-1370.
33. Stalker TJ, Traxler EA, Wu J, et al. Hierarchical organization in the hemostatic response and its relationship to the platelet-signaling network. *Blood.* 2013;121(10):1875-1885.
34. Falati S, Gross P, Merrill-Skoloff G, Furie BC, Furie B. Real-time in vivo imaging of platelets, tissue factor and fibrin during arterial thrombus formation in the mouse. *Nat Med.* 2002;8(10): 1175-1181.